https://www.scirp.org/journal/jbise
J. Biomedical Science and Engineering,
2024, Vol. 17, (No. 6), pp: 107-128

From Simulation to Reality: A Comprehensive Study on the Efficacy of a Rotating Monopolar and Bipolar Radiofrequency System through *In-Silico* Modeling and Pre-Clinical and Clinical Validation

Gregorio Viera Mármol, Ana Lorena Urbano Bojorge, Alicia Robledo Jorge, José Antonio Ferrández Martínez, Olalla Calvo Lozano

High Technology Products S.L.U. (Sinclair), Barcelona, Spain

Correspondence to: Gregorio Viera Mármol, gregorioviera@sinclair.com; Ana Lorena Urbano Bojorge, lurbano@sinclair.com; Alicia Robledo Jorge, arobledos@sinclair.com; José Antonio Ferrández Martínez, jferrandez@sinclair.com; Olalla Calvo Lozano, ocalvo@sinclair.com

Keywords: Comsol Multiphysics Simulations, Radiofrequency Skin Tightening, Fat Reduction, Body Contouring, Cellulite

Received: April 22, 2024 **Accepted:** June 23, 2024 **Published:** June 26, 2024

ABSTRACT

Background: Skin aging is an unavoidable process aggravated by environmental agents. Among other energy devices, non-invasive radiofrequency (RF) technology is widely used for skin tightening and body contouring as it is simpler and more affordable than other technologies that also minimize pain and side-effects. However, most of the current RF devices do not provide automatic skin temperature control and it is difficult to achieve controlled, deep, and harmless thermal increase, so treatment performance and safety is dependent on the operator's movements and expertise. Objective: To show the potential of numerical simulations for optimizing the design of monopolar and bipolar RF electrodes that are capable of providing homogeneous, deep and controlled heating. Materials and methods: *In-silico* models were developed and analyzed using Comsol Multiphysics software to simulate the RF effect produced in tissue by rotating monopolar and bipolar electrodes with different geometries from the Sculpt & Shape RF device (Sinclair, Spain), operating at frequencies of 0.5 and 1 MHz. *Ex-vivo* and *in-vivo* proof-of-concept tests were carried out to validate the simulations. Finally, treatments were performed on 16 subjects and a total of 78 body areas to assess the clinical results generated by the RF electrodes for skin tightening and body contouring. Results: *In-silico* studies emulated the superficial and deep dispersion of heat due to the release of RF energy into human skin tissue. The rotating

electrodes (monopolar and bipolar) and the selected RF frequency (0.5 and 1 MHz) determined the homogeneity of the thermal distribution, the penetration depth (between 4.37 mm and 25.0 mm) and the heating dynamics (between 30 and 100 seconds to reach the target skin temperature), which were confirmed by *ex-vivo* and *in-vivo* tests. In addition, real treatments on facial and body areas using skin temperatures of between 43˚C and 44˚C showed consistent results with good clinical efficacy for skin tightening, circumference reduction and cellulite reduction, with no adverse effects and high subject satisfaction. Conclusions: New monopolar and bipolar RF electrodes with rotating technology have been designed and optimized using numerical simulations. The use of *in-silico* studies and accurate models that reproduce the thermal behavior of human biological tissues can be used to better understand RF devices and to develop superior, efficient, and safer products more quickly.

1. INTRODUCTION

Collagen and elastin are the most relevant proteins that support the connective tissue of the skin, providing elasticity and a desirable appearance [1, 2]. The loss of these proteins is an undesirable process that results in clinical manifestations such as wrinkles, skin sagging and laxity since the skin becomes thinner and loses elasticity [1]. Aging of the skin or skin elastosis can be aggravated by genetic and environmental factors such as chronic exposure to ultraviolet radiation, smoking, air pollution and diet [3]. Traditionally, skin deterioration has been treated with invasive surgical procedures [4-6] which involve a certain risk for the subject during surgery, recovery time, post-operative care and side effects such as pigmentation. In addition, these invasive surgical treatments usually have a high financial cost.

Energy-based devices emerged as excellent candidates for performing skin treatments in a non- or minimally invasive manner. As the first candidates, non-ablative [7] and ablative [8, 9] lasers have been widely used in the aesthetic medicine sector, although their popularity has declined due to the complications associated with their difficulty of use and the side effects caused by absorption in the different skin chromophores [10]. From this situation, novel energy-based devices that use energy sources other than light have emerged, such as radiofrequency (RF) [11, 12]. RF technology has been found to provide optimal results through a technique that is simpler and more affordable for both clinicians and subjects, while also minimizing pain and side-effects and shortening recovery time [13, 14].

RF energy was first employed for therapeutic uses in the 1920s when Bovie developed a prototype electrosurgical instrument [15]. For more than a century, RF devices have been widely used in several medical fields, ranging from control of intra-atrial re-entrant tachycardia [16] to minimally invasive tissue destruction [17, 18] and pain reduction [19]. In the aesthetic medicine field, RF technology can be used to address skin elastosis, photoaging, cellulite or localized fat, among other medical and aesthetic indications [20, 21].

An RF device produces electrical energy at frequencies ranging from 3 Hz to 300 GHz. When the electrical current passes through the different tissues, it generates heat due to the electrical resistance (impedance) of the tissues themselves. The heat induces mechanical and biochemical reactions that affect the skin and the subcutaneous tissue. These biological effects include 1) vasodilatation [22]; 2) contraction of skin fibers, thereby increasing blood circulation and cellular oxygenation stimulation of the lymphatic system [23, 24]; 3) collagen remodeling [25, 26]; 4) fibroblast stimulation, producing new collagen and elastin and improving the extracellular matrix of the skin [27, 28]; 5) increased adipocyte metabolism [21, 29]; and even 6) the induction of adipocyte apoptosis [30]. In summary, RF primarily produces three effects: increased blood microcirculation, increased elasticity of connective tissue in the dermis, and shrinkage of fat cells in the subdermal tissue. In terms of the visual effect in subjects, RF produces skin tightening, a lifting effect and body contouring [31].

Unlike lasers, RF energy is not absorbed by skin chromophores and skin melanin, allowing it to be used safely on all skin types [32]. However, to ensure a completely safe and efficient effect of RF on the skin, a temperature of between 39˚C and 43˚C must be maintained for 5 - 10 minutes [25, 26]. It is generally advised to not exceed 45˚C and to use a limited time period to avoid any thermal injuries to the skin [33].

There is a wide variety of RF medical-aesthetic devices on the market that, based on the RF electrode configurations, can be classified as 1) unipolar [34]; 2) monopolar [35]; 3) bipolar [22]; 4) multipolar [36]; or 5) fractional [32, 37]. Most of these are considered non-invasive devices, except the fractional type which generates coagulation effects and tissue ablation. Among non-invasive medical-aesthetic RF devices, the most used and studied in the literature are the monopolar variety, where one electrode is in contact with the skin and the other serves as a grounding pad [38], and the bipolar variety, which incorporate two or more rows of parallel electrodes in the same applicator [39]. Electrode size and geometry are paramount for RF penetration [39], increasing in the bipolar type with the distance between the electrodes, and in the monopolar type with the size of the electrodes [12, 25]. Other important parameters for RF release are the electrical impedance of the tissue [38, 40], the RF power delivered, and the exposure time [11, 41]. In addition, the penetration depth of RF energy is inversely proportional to the square root of the frequency [22].

During RF application, two modes are used: static and dynamic. Static or stamping mode produces a high peak skin temperature with a short exposure time, and most of these devices employ contact cooling to prevent skin damage [35]. Great skin tightening results have been reported [20, 41]; however, these can be limited by pain and a high risk of burns and other side effects. On the other hand, dynamic or continuous mode produces a lower peak skin temperature and uses a longer exposure time by performing multiple passes over the treatment area [25], which is found to reduce pain and side effects.

Despite RF being a well-established technology that has been implemented in the market, these non-invasive devices present some limitations [40]. Most RF devices do not have an automatic temperature control system [42] and the heat is concentrated around electrodes which may lead to hot spots and non-uniform heating. The physicians must set the RF power, monitor the skin temperature and perform constant movements to provide more uniform and comfortable heating in accordance with the subject's pain threshold and skin reaction. Consequently, treatment is highly dependent on professional experience and praxis. Otherwise, electric arcs can be produced when the contact between the RF electrode and the tissue is not suitable (on uneven body contours or due to irregular applicator lifting), causing severe skin damage [29, 43]. The use of capacitive electrodes versus resistive ones has been found to solve this limitation, but these RF devices may have less efficacy due to higher impedance [44]. Additionally, some RF devices incorporate vacuum suction systems in the handpieces [36]. Although the efficacy of energy delivery is controlled and optimized through the suction, the treatment time becomes longer.

The development, implementation and improvement of RF systems is typically constrained by a lack of knowledge about proper heating inside the tissue. Traditionally, heat dispersion is evaluated indirectly through pre-clinical and clinical studies at the final stages of device validation. However, these studies are not only time consuming but also costly. The use of engineering and mathematical tools in the early stages of RF device development would optimize the process by reducing time and improving the understanding of the application for better efficacy and safety. *In-silico* studies have proven to be an efficient tool in biomedical applications, particularly when measuring internal parameters of the human body is only possible using invasive methods [45] or when a priori understanding of the results of new designs is needed [46]. Recently, numerical simulations have been used to design other energy-based devices such as lasers and cryolipolysis tools for aesthetic indications [47, 48]. In this study, the full development and implementation of a novel RF device with rotative electrodes for medical-aesthetic purposes is described. The presented study spans the whole process from the *in-silico* design and study of monopolar and bipolar RF electrodes using COMSOL Multiphysics, right through to the clinical validation. This research aims to show the potential of *in-silico* studies to optimize RF device design. Numerical simulation provides precise insights into heat behavior (uniformity and depth) in human tissue, enabling more accurate and straightforward device fabrication.

2. MATERIALS AND METHODS

2.1. Radiofrequency Device

Sculpt & Shape® (Sinclair, Spain) is a non-invasive RF device for skin tightening, body contouring and cellulite treatments. Among others, this device is equipped with three tips (Figure 1), whose technical characteristics are detailed in Table 1.

The RF tips include a 360˚ rotating technology to provide homogeneous heating and massage the tissue. The rotation speed for all electrodes is 40 rpm. Likewise, the target skin temperature can be configured between 39˚C and 45˚C for five treatments (wrinkles, facial skin tightening, body skin tightening, cellulite, and body shaping). A real-time temperature and impedance measurement system regulates RF power to achieve the target temperature and maintain it until the end of the treatment, or temporarily cut off the power delivery in the event of no contact between the skin and the electrode.

2.2. *In-Silico* Study

The RF tips were modeled, simulated and optimized using COMSOL Multiphysics® software (version 5.4, COMSOL Inc., Burlington, MA). The tips had been designed previously with SolidWorks® software (SolidWorks Corp., Massachusetts) and then imported to COMSOL Multiphysics. Several iterations of testing and improvement were performed. This study shows the final version of the design.

2.2.1. Model Geometry

The simulations recreated the application of RF electrical currents to a specific area of the body with rotational movements.

The meshed geometrical domains consisted of the biological tissues (dermis and adipose tissue) and the RF tip in contact with the tissue (Figure 2). The thickness of the skin and fat layers were 2.75 and 46.25 mm, respectively, for monopolar electrodes, and 4 and 51.5 mm for bipolar electrodes.

To present the results of the thermal maps, the XY-plane cut (Figure 2) was employed to determine the depth of heat penetration into the tissue and the XZ-plane cut (Figure 2) was used to show the superficial heat on the tissue.

The tips incorporate a rotating movement, which is implemented in the simulations through a deformed geometry feature. However, the translational movement that the operator would perform on the body area was not implemented.

Figure 1. Monopolar and bipolar RF electrodes used in this study.

Table 1. Technical characteristics of the tips.

Tip	Description of electrode	Type of RF	Frequency (MHz)
Shine	Spherical anodized aluminum	Monopolar	1
Firm	Rectangular and flat anodized aluminum	Monopolar	1
Sculpt6	Concave surface with 2 rows of 3 spherical stainless-steel electrodes	Bipolar	0.5

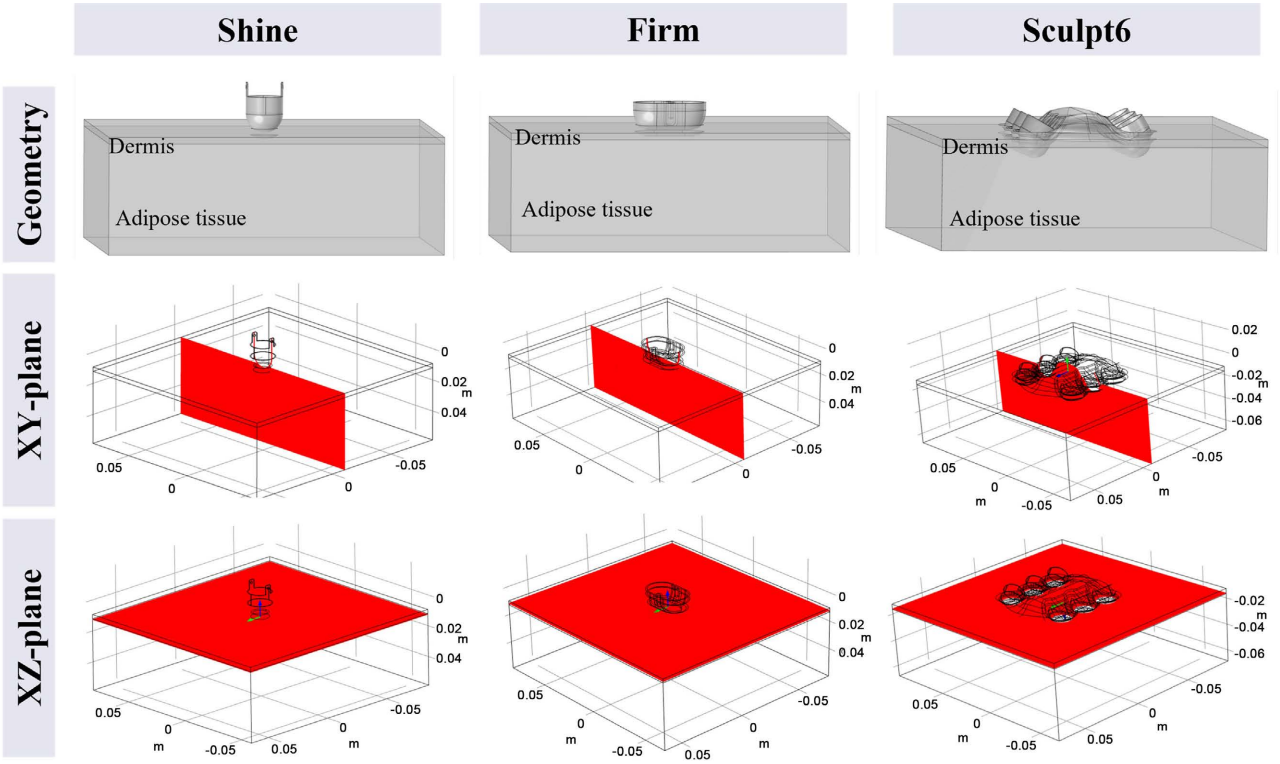

Figure 2. Geometrical layout of the *in-silico* model which consists of electrode, dermis and adipose tissue, as well as XY and XZ planes.

2.2.2. Physics and Thermal Equations

The equations used for the numerical simulations (dynamic electric currents, electrostatics, electromagnetic heating and bioheat transfer module) are included in **Section 1.1 Supplementary Information (SI)**. Additionally, this section incorporates tables indicating the thermal parameters of the tissues and materials (Table S1), the electrical parameters of the tissues and materials (Table S2), and the thermal and perfusion parameters of the blood (Table S3).

2.2.3. Boundary Conditions

All information is provided in Section **1.2 SI**.

2.2.4. Mesh Generation

All information is provided in Section **1.3 SI**.

2.3. *Ex-Vivo* Study. Proof of Concept Tests

The simulated results of heating inside the tissue (XY planes in Figure 2) were compared with the results obtained with pig tissue (Figure S1). Pork belly pieces without the superficial skin and with an initial temperature of 15˚C to 20˚C were used.

The pieces of pig tissue were measured and cut to ensure uniform size and thickness. In addition, the pieces used with the bipolar electrode were sliced in half to compare the same plane as the simulations. A thin layer of glycerin gel[1] was spread across the surface of the tissue touching the RF tip to improve contact.

The monopolar electrodes were evaluated in rotating mode. However, the bipolar electrode was used without rotation to avoid damaging the pig tissue during the test.

[1]Sinclair internal reference: 100017252.

Thermal measurements were taken using a Ti200 infrared thermal imaging camera (Fluke Corp, Washington). It was placed in front of the tissue that was used to obtain cross-sectional temperature maps and determine the depth of heat penetration inside tissue. The experiments were performed at room temperature and carried out by the same person to avoid variations in the force applied to the tissue. A minimum of five independent experiments were conducted.

Thermal images were analyzed using Fluke Connect software (Fluke Corp, Washington). An isotherm area of 5˚C under the maximum temperature was considered to calculate the penetration depth of the heat inside the pig tissue. ImageJ software (National Institutes of Health, Maryland) was employed to convert pixels on the thermal image into millimeters of tissue. Data analysis was performed using Microsoft Excel 365 (Microsoft, New Mexico) and data were presented as Mean ± Standard Deviation.

2.4. *In-Vivo* Study. Proof of Concept Tests

The simulated results for surface heating (XZ planes in Figure 2) were compared with the results obtained from skin heating measurements conducted on facial and corporal areas. A total of 6 facial areas were heated with the monopolar Shine tip, 9 facial areas with the monopolar Firm tip, 10 corporal areas with the Sculpt6 tip at 0.5 MHz, and 9 corporal areas with the Sculpt6 tip at 1 MHz. All subjects who participated in the study were previously briefed and signed a consent form.

The skin was cleaned with mild soap and water. A thin layer of glycerin gel was then applied. No topical anesthesia was applied before the treatment. The target temperature was 42˚C. During the test, the handpiece was constantly moved in a uniform pattern to achieve a homogeneous heat while remaining in full contact with the body area being treated.

All tips have an internal infrared sensor that measures the temperature in real time. The data obtained was stored in the device's memory and later extracted for analysis.

The times taken to reach the set temperature were compared. The sets of values obtained for each case were compared with the results obtained from the corresponding simulation.

2.5. Clinical Validation

The inclusion criteria included males and females between 18 and 75 years old with concerns about skin laxity, wrinkles, cellulite, or localized fat. Specific exclusion criteria included active dermatological disease or infectious processes in the treatment area; pregnancy; breastfeeding; implanted electronic devices; blood disorders or the use of blood-thinning or antiplatelet medications; a history of active or recent neoplastic malignancy; heat-stimulated conditions and orthopedic surgery such as replacement of the hip, femur, etc.

A total of 16 subjects (14 women and 2 men) were willing to be treated for skin tightening, body shaping, wrinkles, and improvement of the appearance of cellulite in sessions performed on both sides of the face, the neck, the décolletage, the abdomen, the legs, the buttocks, and the flanks. A total of 78 areas underwent treatment. 31 areas were treated with the Sculpt6 tip to address cellulite reduction and body shaping, 25 areas were treated for skin tightening using the Firm tip, and 22 areas were treated for wrinkles with the Shine tip.

Subjects were not required to follow a special diet or exercise plan. Prior to treatment, all subjects received a detailed and clear explanation of the planned procedure and signed an informed consent form. The complete confidentiality of the subjects' data was guaranteed throughout the entire process.

2.5.1. Protocol

Anthropometric data (sex, age, body weight and height) were recorded. Photographs at 45˚ and 90˚ angles, as well as frontal and lateral views of the treatment area, were taken at every visit before starting the procedure.

Glycerin gel was applied to the treatment areas and no anesthesia was required. The applicator was continuously moved according to the direction of the lymphatic system to achieve homogeneous and gra-

dual heating of the area while maintaining contact with the skin. The target temperature for the treatments was determined to be between 43˚C and 45˚C, depending on the subject's tolerance. The device automatically regulated the RF power to maintain a constant temperature throughout the treatment.

Treatments were performed every 1 or 2 weeks. Facial sessions lasted between 12 and 40 minutes, while body sessions, depending on the areas treated, lasted between 20 and 60 minutes. Details of the clinical treatments are shown in Table S4. All treatments were performed in accordance with the treatment tables recommended by the manufacturer.

2.5.2. Efficacy and Safety Evaluation

Improvements in the appearance of skin texture and body contouring compared to baseline photographs were rated by three blinded and experienced researchers, who carried out the evaluation on each pair of pre- and post-treatment photographs. The Global Aesthetic Improvement Scale with a 0 to 4 range (0 = no improvement; 1 = mildly improved; 2 = improved; 3 = much improved; 4 = very much improved) was used. Likewise, subject satisfaction was evaluated on a 0 to 3 scale (0 = unsatisfied; 1 = low satisfaction; 2 = satisfied; 3 = very satisfied) 1 month after the last treatment.

Also, the safety was evaluated by asking the patients their perception of pain/heat during the treatment, through a scale with a 0 to 10 range (0 no pain, 1-4 mild pain, 5-7 moderate pain, 8-10 severe pain). Adverse effects are also reported during each session.

2.5.3. Statistical Analysis

A student's two-tailed paired t-test was applied to assess the statistical significance of the efficacy evaluation. A probability value of 95% ($p < 0.05$) was considered statistically significant. Data were analyzed using Microsoft Excel 365.

3. RESULTS

3.1. Comparison between Simulations and *Ex-Vivo* and *In-Vivo* Tests

3.1.1. Monopolar Electrodes

The thermal images taken of the skin of a subject during a real treatment were shown to be very similar to the simulation of the rotating tips. However, in the case of the Firm applicator, due to its rectangular shape, the absence of rotation generated a rectangular thermal image, which is transformed into circular heating when the tip rotates (Figure 3).

The temperature scales may differ between simulation and real treatment due to the difference between the initial values of the skin and ambient temperatures.

The heating inside the tissue has also been found to be very similar between the tests carried out with pig tissue and the simulations (Figure 4). An isotherm of 5˚C, from 44˚C to 39˚C (thin black line in the simulations) was drawn to calculate the heat penetration depth (Table 2).

3.1.2. Bipolar Tip

The effect of rotation is more notable in the case of the bipolar tip. Without rotation, all the heat is concentrated under the electrodes, while rotation homogenizes the heat under the tip (Figure 5).

Table 2. Penetration depth calculations from *ex-vivo* tests and simulations using the monopolar electrodes.

Tip	Penetration depth (mm)	
	Pig tissue	Simulation
Shine	4.69 ± 0.96	4.37
Firm	6.80 ± 1.63	10.58

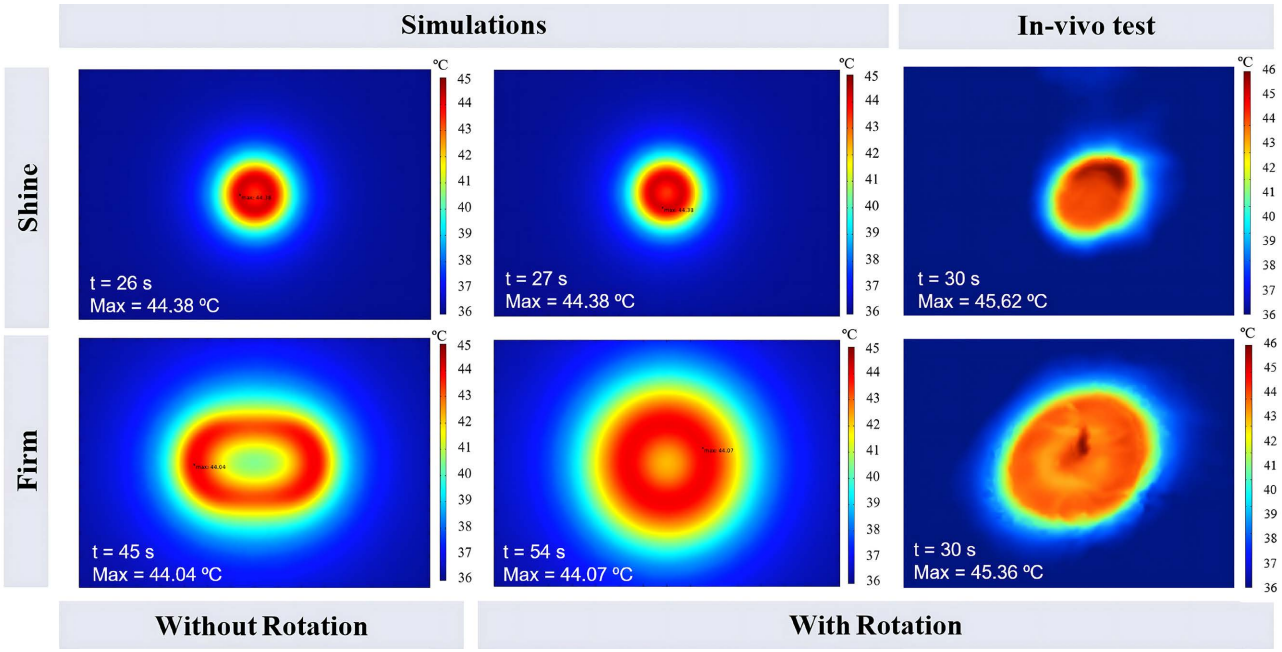

Figure 3. Surface thermal maps from simulations and a subject's skin using monopolar electrodes, with and without rotation. The time to reach maximum temperature for each test and simulation is shown.

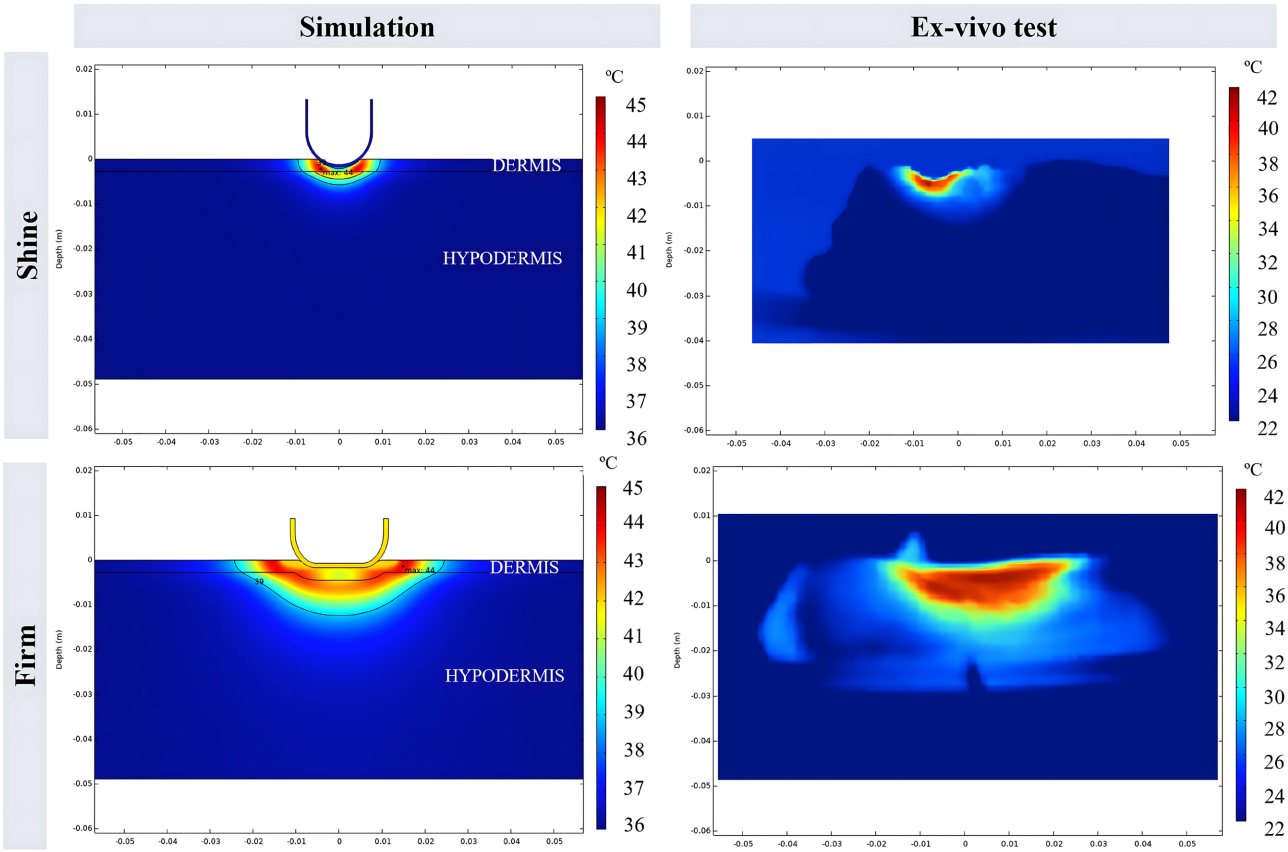

Figure 4. Heat penetration depth simulated (left) and measured in *ex-vivo* pig tissue using monopolar electrodes (right).

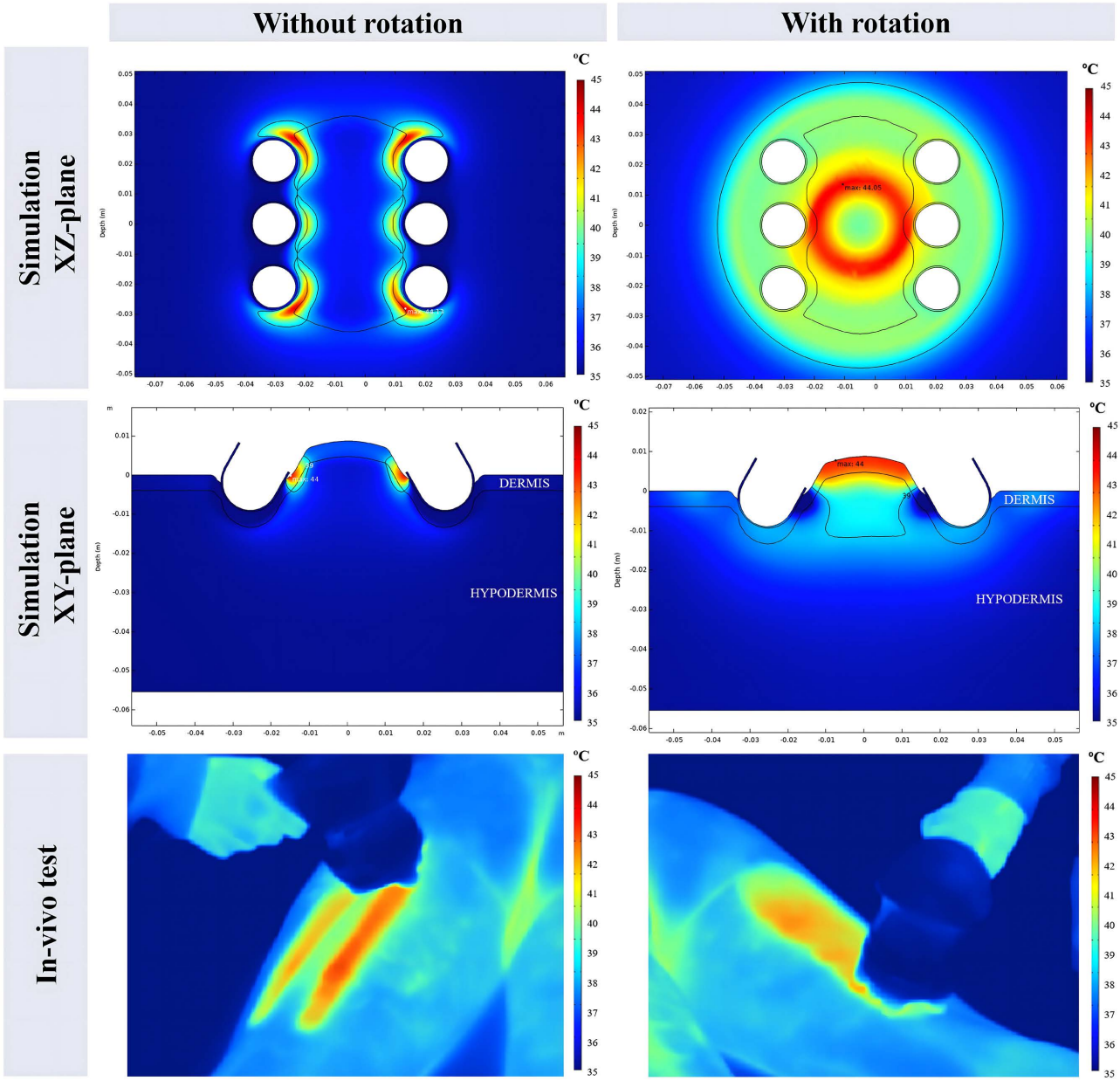

Figure 5. Comparison of heat distribution with and without bipolar tip rotation. Results from simulations in the XY and XZ shear planes and testing on a subject.

The effect of frequency with the bipolar applicator is shown in Figure 6. The penetration depth simulated for 0.5 MHz was 25.00 mm, and for 1 MHz it was 20.15 mm.

Ex-vivo tests with pig tissue could not be performed with rotation because the tissue was damaged and did not allow for reliable results. Without rotation, heating was concentrated under the electrode (Figure 7), as shown by the tests conducted on the surface (Figure 5). Qualitatively, a greater penetration depth was also observed with the lowest frequency of 0.5 MHz.

3.1.3. Heating Dynamics

Figure 8 compares the times required by each tip to reach the set temperature (42˚C for these tests), which were obtained from the simulations and in tests with subjects. For each tip, a set of *in-vivo* tests was

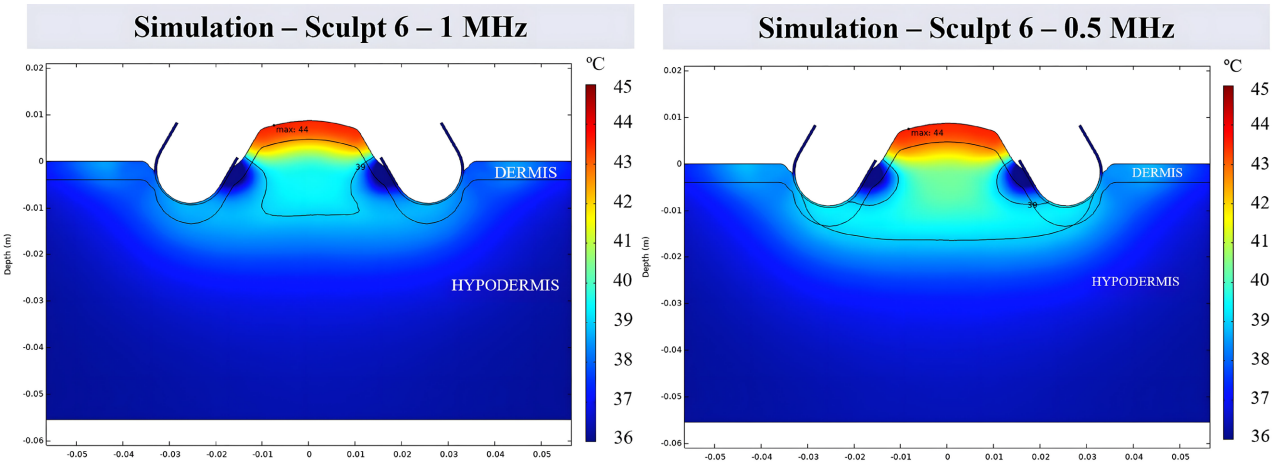

Figure 6. Thermal distribution of the simulation result with the bipolar tip. XY-plane is shown with rotation.

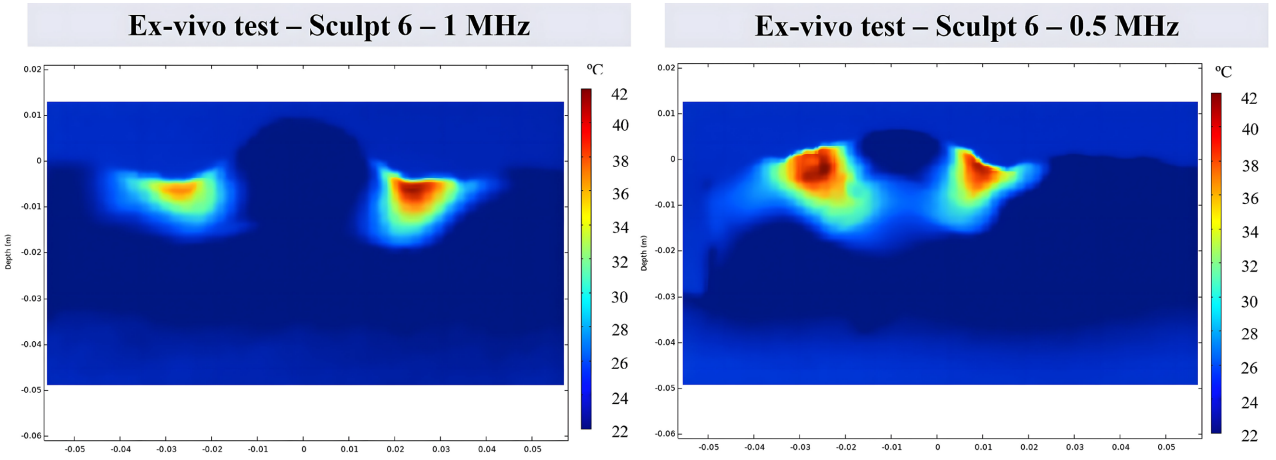

Figure 7. Thermal distribution of the test on pig tissue with the bipolar tip. The rotation of the tip was not activated.

performed to provide a statistic which is compared with the single value obtained in the simulation. Monopolar electrodes took around 30 s to reach 42˚C, and about 100 s for bipolar one.

3.2. Clinical Validation

All subjects completed at least 7 sessions of RF treatments, with an average treatment time of 18 minutes for facial treatments and 40 minutes for body treatments; the treatment temperature range was 42 to 44˚C. Information related to the treatments and the characteristics of the subjects is presented in Table S4. Before and after images of representative treatments are shown in Figure 9.

The clinical investigators' assessment using the GAIS resulted in a score of 1.83 out of 4, which is a 25% - 49% improvement over baseline. Moreover, subject satisfaction after 1 month was evaluated through personal questionnaires, which reported a value of 2.50 out of 3 (between satisfied and very satisfied). No side or adverse effects were reported.

The subjects rated the heat/pain experienced from the heating during the treatment at 6.6 ± 1.1 on a scale of 1 to 10. Minor adverse effects were observed, such as mild superficial first-degree burns (which disappeared within a few days) resulting from sparks due to the tip losing contact with the skin during treatment sessions. No major adverse effects were reported.

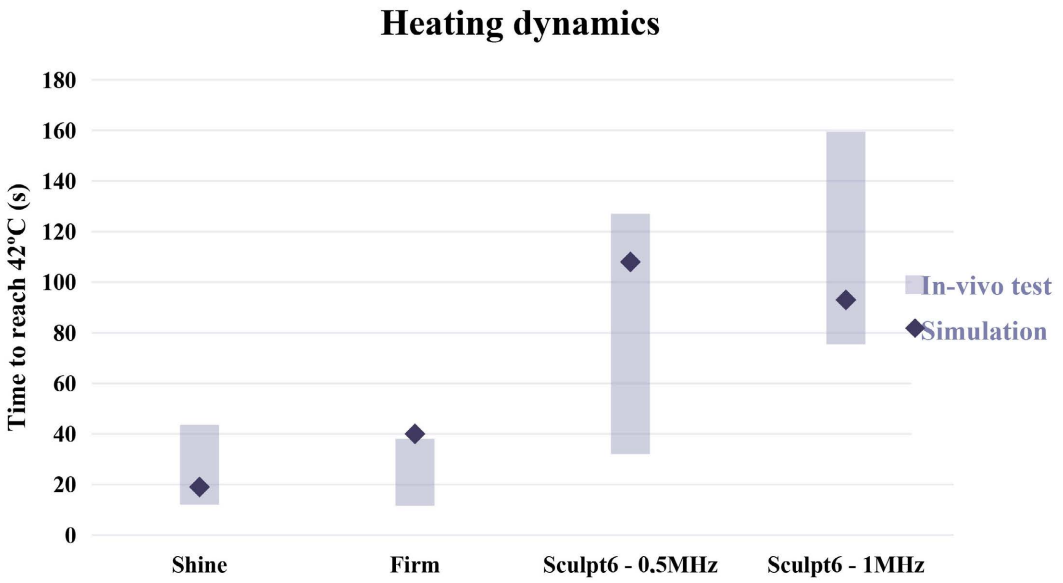

Figure 8. Heating dynamics. Time ranges to reach 42˚C measured in *in-vivo* tests and the simulated values for each tip.

Patient A (Female, 43): 8 sessions of skin tightening on face with Shine and Firm tips (1 MHz) at 44ºC. There is a decrease in frontal and periocular expression lines, and in marionette lines.

Patient B (Female, 47): 8 sessions of skin tightening on face with Shine and Firm tips (1 MHz) at 44ºC. Improvement on skin quality, texture and tightening on submental area and cheeks.

Patient C (Male, 28): 8 sessions of body shaping on flanks and abdomen with Sculpt6 tip (0,5 MHz) at 44ºC. Circumference and fold: -2cm.

Patient D (Female, 52): 9 sessions of cellulite on legs with Sculpt6 tip (1 MHz) at 44ºC. Improvement of skin texture and reduction of cellulite.

Figure 9. Before and after treatment images. (A) and (B) face skin tightening treated with monopolar electrodes, (C) body shaping and (D) cellulite, both treated with a bipolar tip.

4. DISCUSSION

The design of devices whose function is to obtain effects on humans is complex. In most cases, the effect is not observable and clinical tests are needed, which can be time consuming, expensive and risky for the individual since these devices are in the testing phase. It is normal for the results to not be optimal, and several stages of redesign and new tests are necessary, making the clinical validation process a long and very expensive one. In general, manufacturing companies opt for designs that replicate other existing products to ensure results and save time, which leads to very similar products and a sector with little innovation.

Simulation tools have been widely used in many sectors, such as electronics, mechanics, fluids, construction, automotive, aeronautics, robotics, and others, which has enabled much faster progress than in the medical sector, for example. This drastically reduces development times from years of trial and error to just a few months. And most importantly, allows for increased understanding and knowledge, as well as taking advantage of the time to innovate and introduce notable improvements in the new products.

The device presented in this study incorporates important innovations for the sector, such as the automatic rotation of the electrodes, which represents a considerable challenge since it compromises contact with the skin, which is essential to transmit the radiofrequency energy and produce the desired movement and heating effect. The aim was to treat the skin and fat in different areas of the face and body in a comfortable, safe, and effective way. Another objective was to provide a mechanical massage to promote lymphatic drainage and enhance the heating effect. Some of the questions that were raised included: What is the optimal geometry of the electrodes? Which technology is more appropriate, monopolar or bipolar? What parameters should be chosen for RF power and frequency? What materials should be used?

Numerical simulations allow for a rapid trial-and-error process, thanks to which a theoretically ideal design can be achieved that is then tested with real patients with a high probability of delivering the expected performance.

In this study, the thermal behavior of RF electrodes from the Sculpt&Shape device equipped with a 360˚ rotation system has been simulated with COMSOL Multiphysics software. The RF tips have been designed and optimized for treatments for different face and body areas and indications. The results of these simulations have been compared with *ex-vivo* and *in-vivo* experiments. The authors had previously used simulations with cryolipolysis and laser hair removal devices [48, 49].

For the facial area, monopolar electrodes have been designed with different sizes and shapes to treat both small areas, to achieve more superficial effects, as well as larger areas, to reach the deeper dermis. Monopolar technology and capacitive materials have been chosen because bipolar technology and resistive materials present a high risk of causing electric arcs due to loss of contact. The effect of RF frequency has also been studied, and a frequency of 1 MHz has been chosen for facial treatments because it is optimal for the depth of the facial skin. A lower frequency would heat deeper areas and may cause an undesirable effect on facial fat (the so-called skeleton face effect). The penetration depth obtained with the smaller electrode (Shine) was 4.37 mm, while the Firm electrode achieved 10.58 mm (**Table 2**). This is in line with the expectation that the monopolar applicator with a larger surface area would achieve a greater depth of penetration. Therefore, the Shine tip has been found to be more suitable for treating fine lines and small areas of the face, while the Firm tip would be used for larger areas and to achieve a deeper effect. It is worth mentioning that for the Shine tip, the results of the simulations and *ex-vivo* measurements were very similar. This is because the Shine tip is small and spherical in shape and when performing the test with the rotating tip, its center could be positioned at the edge of the pig tissue. On the other hand, due to the flat and rectangular shape of the Firm applicator, the center of the applicator was not on the edge of the tissue and therefore the cutting planes of the simulation and the pig tissue did not coincide. Beyond the variation values, the simulation provided relevant information regarding heat dispersion inside the tissue and possible biological effects.

For the body area, the objective with the design of the RF tip was to also reach the hypodermis and provide a mechanical massage. A ball-based design and a concave cavity were chosen, which were opti-

mized through simulation to treat large areas, achieve homogeneous heating, and offer a mechanical massage for improved comfort and effectiveness. To increase RF power transmission, resistive materials were chosen. Electric arcs have been suppressed by a real-time impedance measurement system that detects a lack of contact and momentarily cuts off the power. In addition, the effect of the RF frequency has been studied and a frequency of 0.5 MHz was determined for treatments whose target is localized fat, while 1 MHz was determined for skin treatments. Especially with bipolar applicators, the simulation has clearly shown the heating homogenization effect introduced by the rotation of the electrodes and how the absence of rotation produces very localized heating around the electrodes, which can cause hot spots and compromise the safety of the treatment (**Figure 3**). This uniform heating, both superficial and internal, ensures that treatments involving subjects are carried out in a safe manner, avoiding hot spots that can be painful and even lead to thermal injuries. This result, together with the internal RF power control of the equipment, allows for repeated treatments where the temperature can be maintained at therapeutic values during the indicated times to achieve the expected biological effects. Moreover, the simulations have demonstrated that heat penetrates deeper at 0.5 MHz than at 1 MHz, as widely reported in the literature [11, 22]. The simulated heat penetration depths obtained by the bipolar tip at 0.5 and 1 MHz were 25.00 mm and 20.15 mm, respectively.

Monopolar applicators usually provide deeper heating than bipolar applicators [50]. However, the bipolar applicator shown in this study produces deeper heating. This is due to its larger size and concave shape, which allow the tissue to be introduced into the applicator and for deeper layers to be targeted.

The results of the heating dynamics were also analyzed. Here, the tests on real subjects have shown a high dispersion, because there are many variables that influence RF power transmission into the tissue, such as the amount of gel used, the way the applicator is moved and pressed into the skin, and the characteristics of the human tissue. These variables affect the time needed to reach the target temperature during a treatment. However, the simulation tissue has fixed parameters and moreover no translational movements were considered. The significance of this study lies in the finding that both the simulations and the measurements taken during treatments have determined shorter times for the monopolar applicators, on average around 30 seconds, and longer times for the bipolar applicators, around 100 seconds.

The functionality of these applicators has been validated with the results shown in this study and with other studies carried out in external clinics [51].

The design and optimization of these three distinct electrodes tailored for specific face and body areas and skin layers demonstrate a thoughtful approach to treatment customization. This versatility is likely to contribute to the device's effectiveness across a range of applications, addressing the diverse needs of subjects and clinicians alike. A commitment to creating a new device that ensures comfortable, efficient and safe treatments is essential.

5. CONCLUSIONS

This research has shown that the use of *in-silico* studies is able to reproduce the thermal behavior of human tissues, thereby providing an increased level of know-how of RF devices and optimizing and accelerating the design and fabrication processes.

The optimization of the Sculpt & Shape® novel RF rotative device has been described. *In-silico* studies performed with COMSOL Multiphysics software provided relevant information about the performance of the RF tips. The results showed the superficial and deep homogeneous dispersion of heat due to the release of RF energy into human skin tissue.

Ex-vivo studies performed on pig tissue for depth penetration analysis, *in-vivo* tests with individuals for superficial temperature evaluations, and finally, real treatments, have confirmed the outcomes of the simulations considering certain limitations associated with the differences between a simulation and a real case.

CONFLICTS OF INTEREST

The authors have no conflicts of interest directly relevant to the content of this article.

ETHICS DECLARATION

This experiment was conducted in accordance with the Declaration of Helsinki, and informed consent was obtained from the participants after they were given a thorough explanation of the main purpose and methods of the experiment both orally and in writing prior to the experiment.

REFERENCES

1. Uitto, J. (1979) Biochemistry of the Elastic Fibers in Normal Connective Tissues and Its Alterations in Diseases. *Journal of Investigative Dermatology*, **72**, 1-10. https://doi.org/10.1111/1523-1747.ep12530093
2. Halper, J. and Kjaer, M. (2014) Basic Components of Connective Tissues and Extracellular Matrix: Elastin, Fibrillin, Fibulins, Fibrinogen, Fibronectin, Laminin, Tenascins and Thrombospondins. *Advances in Experimental Medicine and Biology*, **802**, 31-47.
3. Kammeyer, A. and Luiten, R.M. (2015) Oxidation Events and Skin Aging. *Ageing Research Reviews*, **21**, 16-29. https://doi.org/10.1016/j.arr.2015.01.001
4. Pitanguy, I. and Machado, B.H.B. (2012) Facial Rejuvenation Surgery: A Retrospective Study of 8788 Cases. *Aesthetic Surgery Journal*, **32**, 393-412. https://doi.org/10.1177/1090820x12438895
5. Blum, C.A., Sasser, C.G.S. and Kaplan, J.L. (2013) Complications from Laser-Assisted Liposuction Performed by Noncore Practitioners. *Aesthetic Plastic Surgery*, **37**, 869-875. https://doi.org/10.1007/s00266-013-0153-x
6. Pereira-Netto, D., Montano-Pedroso, J.C., Aidar, A.L.e.S., Marson, W.L. and Ferreira, L.M. (2018) Laser-Assisted Liposuction (LAL) versus Traditional Liposuction: Systematic Review. *Aesthetic Plastic Surgery*, **42**, 376-383. https://doi.org/10.1007/s00266-018-1085-2
7. Sadick, N.S. (2003) Update on Non-Ablative Light Therapy for Rejuvenation: A Review. *Lasers in Surgery and Medicine*, **32**, 120-128. https://doi.org/10.1002/lsm.10127
8. Hruza, G.J. (1996) Laser Skin Resurfacing. *Archives of Demartological Research*, **132**, 451-455. http://archderm.jamanetwork.com/
9. Tanzi, E.L., Lupton, J.R. and Alster, T.S. (2003) Lasers in Dermatology: Four Decades of Progress. *Journal of the American Academy of Dermatology*, **49**, 1-34. https://doi.org/10.1067/mjd.2003.582
10. Nanni, C.A. and Alster, T.S. (1998) Complications of Cutaneous Laser Surgery. A Review. *Dermatologic Surgery*, **24**, 209-219. https://doi.org/10.1111/j.1524-4725.1998.tb04139.x
11. Beasley, K.L. and Weiss, R.A. (2014) Radiofrequency in Cosmetic Dermatology. *Dermatologic Clinics*, **32**, 79-90.
12. Bonjorno, A.R., Gomes, T.B., Pereira, M.C., de Carvalho, C.M., Gabardo, M.C.L., Kaizer, M.R., *et al.* (2019) Radiofrequency Therapy in Esthetic Dermatology: A Review of Clinical Evidences. *Journal of Cosmetic Dermatology*, **19**, 278-281. https://doi.org/10.1111/jocd.13206
13. Gold, M., Taylor, M., Rothaus, K. and Tanaka, Y. (2016) Non-Insulated Smooth Motion, Micro-Needles RF Fractional Treatment for Wrinkle Reduction and Lifting of the Lower Face: International Study. *Lasers in Surgery and Medicine*, **48**, 727-733. https://doi.org/10.1002/lsm.22546
14. Alexiades-Armenakas, M., Dover, J.S. and Arndt, K.A. (2008) Unipolar versus Bipolar Radiofrequency Treatment of Rhytides and Laxity Using a Mobile Painless Delivery Method. *Lasers in Surgery and Medicine*, **40**, 446-453. https://doi.org/10.1002/lsm.20667
15. Mclean, A.J. (1929) The Bovie Electrosurgical Current Generator Some Underlying Principles and Results. http://archsurg.jamanetwork.com/
16. Triedman, J.K., Bergau, D.M., Saul, J.P., Epstein, M.R. and Walsh, E.P. (1997) Efficacy of Radiofrequency Ablation for Control of Intraatrial Reentrant Tachycardia in Patients with Congenital Heart Disease. *Journal of the*

American College of Cardiology, **30**, 1032-1038. https://doi.org/10.1016/s0735-1097(97)00252-0

17. Gillams, A.R. (2005) The Use of Radiofrequency in Cancer. *British Journal of Cancer*, **92**, 1825-1829. https://doi.org/10.1038/sj.bjc.6602582
18. Kinney, B.M., Andriessen, A., DiBernardo, B.E., Bloom, J., Branson, D.F., Gentile, R.D., *et al*. (2017) Use of a Controlled Subdermal Radio Frequency Thermistor for Treating the Aging Neck: Consensus Recommendations. *Journal of Cosmetic and Laser Therapy*, **19**, 444-450. https://doi.org/10.1080/14764172.2017.1343952
19. Kumaran, B. and Watson, T. (2019) Treatment Using 448 kHz Capacitive Resistive Monopolar Radiofrequency Improves Pain and Function in Patients with Osteoarthritis of the Knee Joint: A Randomised Controlled Trial. *Physiotherapy*, **105**, 98-107. https://doi.org/10.1016/j.physio.2018.07.004
20. Ruiz-Esparza, J. (2006) Nonablative Radiofrequency for Facial and Neck Rejuvenation. A Faster, Safer, and Less Painful Procedure Based on Concentrating the Heat in Key Areas: The ThermaLift Concept. *Journal of Cosmetic Dermatology*, **5**, 68-75.
21. Mazzoni, D., Lin, M.J., Dubin, D.P. and Khorasani, H. (2019) Review of Non-Invasive Body Contouring Devices for Fat Reduction, Skin Tightening and Muscle Definition. *Australasian Journal of Dermatology*, **60**, 278-283.
22. Belenky, I., Margulis, A., Elman, M., Bar-Yosef, U. and Paun, S.D. (2012) Exploring Channeling Optimized Radiofrequency Energy: A Review of Radiofrequency History and Applications in Esthetic Fields. *Advances in Therapy*, **29**, 249-266. https://doi.org/10.1007/s12325-012-0004-1
23. Bächinger, H.P., Bruckner, P., Timpl, R., Prockop, D.J. and Engel, J. (1980) Folding Mechanism of the Triple Helix in Type-III Collagen and Type-III PN-Collagen: Role of Disulfide Bridges and Peptide Bond Isomerization. *European Journal of Biochemistry*, **106**, 619-632. https://doi.org/10.1111/j.1432-1033.1980.tb04610.x
24. Macdonald, J.R. and Bächinger, H.P. (2001) HSP47 Binds Cooperatively to Triple Helical Type I Collagen but Has Little Effect on the Thermal Stability or Rate of Refolding. *Journal of Biological Chemistry*, **276**, 25399-25403. https://doi.org/10.1074/jbc.m102471200
25. Nelson, A.A., Beynet, D. and Lask, G.P. (2015) A Novel Non-Invasive Radiofrequency Dermal Heating Device for Skin Tightening of the Face and Neck. *Journal of Cosmetic and Laser Therapy*, **17**, 307-312. https://doi.org/10.3109/14764172.2015.1039035
26. Fritz, K., Bernardy, J., Tiplica, G.S. and Machovcova, A. (2015) Efficacy of Monopolar Radiofrequency on Skin Collagen Remodeling: A Veterinary Study. *Dermatologic Therapy*, **28**, 122-125. https://doi.org/10.1111/dth.12195
27. Hiragami, F., Motoda, H., Takezawa, T., Takabayashi, C., Inoue, S., Wakatake, Y., *et al*. (2009) Heat Shock-Induced Three-Dimensional-Like Proliferation of Normal Human Fibroblasts Mediated by Pressed Silk. *International Journal of Molecular Sciences*, **10**, 4963-4976. https://doi.org/10.3390/ijms10114963
28. McGee, M.P., Morykwas, M., Shelton, J. and Argenta, L. (2012) Collagen Unfolding Accelerates Water Influx, Determining Hydration in the Interstitial Matrix. *Biophysical Journal*, **103**, 2157-2166. https://doi.org/10.1016/j.bpj.2012.10.010
29. Weiss, R.A. (2013) Noninvasive Radio Frequency for Skin Tightening and Body Contouring. *Seminars in Cutaneous Medicine and Surgery*, **32**, 9-17.
30. Franco, W., Kothare, A., Ronan, S.J., Grekin, R.C. and McCalmont, T.H. (2010) Hyperthermic Injury to Adipocyte Cells by Selective Heating of Subcutaneous Fat with a Novel Radiofrequency Device: Feasibility Studies. *Lasers in Surgery and Medicine*, **42**, 361-370. https://doi.org/10.1002/lsm.20925
31. Lee, C. and Gold, M.H. (2020) Updates on Radiofrequency Devices for Skin Tightening and Body Contouring. *Dermatological Reviews*, **1**, 75-83. https://doi.org/10.1002/der2.31
32. Seo, K.Y., Yoon, M.S., Kim, D.H. and Lee, H.J. (2012) Skin Rejuvenation by Microneedle Fractional Radiofre-

quency Treatment in Asian Skin; Clinical and Histological Analysis. *Lasers in Surgery and Medicine*, **44**, 631-636. https://doi.org/10.1002/lsm.22071

33. Paul, M., Blugerman, G., Kreindel, M. and Mulholland, R.S. (2010) Three-Dimensional Radiofrequency Tissue Tightening: A Proposed Mechanism and Applications for Body Contouring. *Aesthetic Plastic Surgery*, **35**, 87-95. https://doi.org/10.1007/s00266-010-9564-0
34. Goldberg, D.J., Fazeli, A. and Berlin, A.L. (2008) Clinical, Laboratory, and MRI Analysis of Cellulite Treatment with a Unipolar Radiofrequency Device. *Dermatologic Surgery*, **34**, 204-209. https://doi.org/10.1097/00042728-200802000-00009
35. Abraham, M.T. and Mashkevich, G. (2007) Monopolar Radiofrequency Skin Tightening. *Facial Plastic Surgery Clinics of North America*, **15**, 169-177. https://doi.org/10.1016/j.fsc.2007.01.005
36. Sadick, N.S., Nassar, A.H., Dorizas, A.S. and Alexiades-Armenakas, M. (2014) Bipolar and Multipolar Radiofrequency. *Dermatologic Surgery*, **40**, S174-S179.
37. Hruza, G.J., Taub, A.F., Hruza, G., Forman Taub, A., Collier, S.L. and Mulholland, S.R. (2009) Skin Rejuvenation and Wrinkle Reduction Using a Fractional Radiofrequency System. *Journal of Drugs in Dermatology*, **8**, 259-265. https://www.researchgate.net/publication/24186755
38. Lolis, M.S. and Goldberg, D.J. (2012) Radiofrequency in Cosmetic Dermatology: A Review. *Dermatologic Surgery*, **38**, 1765-1776. https://doi.org/10.1111/j.1524-4725.2012.02547.x
39. Elsaie, M. (2009) Cutaneous Remodeling and Photorejuvenation Using Radiofrequency Devices. *Indian Journal of Dermatology*, **54**, 201-205. https://doi.org/10.4103/0019-5154.55625
40. Malone, C.H., Walters, N., Stroh, R. and Munavalli, G. (2021) New Technologies in Skin Tightening. *Current Otorhinolaryngology Reports*, **9**, 422-435. https://doi.org/10.1007/s40136-021-00371-5
41. Green, J. and Greene, R. (2014) Skin Tightening Technologies. *Facial Plastic Surgery*, **30**, 062-067. https://doi.org/10.1055/s-0033-1363756
42. El-Domyati, M., El-Ammawi, T.S., Medhat, W., Moawad, O., Brennan, D., Mahoney, M.G., *et al.* (2011) Radiofrequency Facial Rejuvenation: Evidence-Based Effect. *Journal of the American Academy of Dermatology*, **64**, 524-535. https://doi.org/10.1016/j.jaad.2010.06.045
43. Harth, Y. and Lischinsky, D. (2011) A Novel Method for Real-Time Skin Impedance Measurement during Radiofrequency Skin Tightening Treatments. *Journal of Cosmetic Dermatology*, **10**, 24-29. https://doi.org/10.1111/j.1473-2165.2010.00535.x
44. Elsaie, M.L., Choudhary, S., Leiva, A. and Nouri, K. (2010) Nonablative Radiofrequency for Skin Rejuvenation. *Dermatologic Surgery*, **36**, 577-589.
45. Kumaran, B. and Watson, T. (2015) Thermal Build-Up, Decay and Retention Responses to Local Therapeutic Application of 448 kHz Capacitive Resistive Monopolar Radiofrequency: A Prospective Randomised Crossover Study in Healthy Adults. *International Journal of Hyperthermia*, **31**, 883-895. https://doi.org/10.3109/02656736.2015.1092172
46. Pšenáková, Z., Šmondrk, M. and Beňová, M. (2015) Modelling and Simulation of the Electricfield Strength Distribution in a Human Head Model by 2,4 Ghz Radiofrequency Radiation. CRC Press.
47. Namakshenas, P. and Mojra, A. (2020) Microstructure-Based Non-Fourier Heat Transfer Modeling of HIFU Treatment for Thyroid Cancer. *Computer Methods and Programs in Biomedicine*, **197**, Article ID: 105698. https://doi.org/10.1016/j.cmpb.2020.105698
48. Mármol, G.V. (2019) New Cooltech Define® Cryoadipolysis Applicators: A Scientific and Comparative Study with Cooltech® Applicators. *Eurasian Journal of Medical Investigation*, **3**, 85-94. https://doi.org/10.14744/ejmi.2019.35267

49. Viera Mármol, G. and Villena, J. (2019) New 3D *in Silico* Model of Hair and Skin Heating during Laser Hair Removal. *International Research Journal of Pharmacy and Medical Sciences* (*IRJPMS*), **1**, 15-24.

50. Viera-Mármol, G., Villena, J., García, P., Khrystova, K. and Colina, M. (2018) A Comparative Study of Cooltech® Handpieces for Cryoadipolysis Using Numerical Simulation. *Problems of Cryobiology and Cryomedicine*, **28**, 343-356. https://doi.org/10.15407/cryo28.04.343

51. Ferrández Martínez, J.A., Viera Mármol, G., Vignoli, F., Perera, J., Blanch, A., Suárez, M., *et al*. (2024) New Rotative Radiofrequency Technology: A Multicenter Retrospective Study on Efficacy and Safety. *Journal of Cosmetics, Dermatological Sciences and Applications*, **14**, 69-83.

52. Durnin, J.V.G.A. and Womersley, J. (1974) Body Fat Assessed from Total Body Density and Its Estimation from Skinfold Thickness: Measurements on 481 Men and Women Aged from 16 to 72 Years. *British Journal of Nutrition*, **32**, 77-97. https://doi.org/10.1079/bjn19740060

53. Lipkin, M. and Hardy, J.D. (1954) Measurement of Some Thermal Properties of Human Tissues. *Journal of Applied Physiology*, **7**, 212-217. https://doi.org/10.1152/jappl.1954.7.2.212

54. Rodríguez de Rivera, P.J., Rodríguez de Rivera, M., Socorro, F., Calbet, J.A.L. and Rodríguez de Rivera, M. (2022) Advantages of *in Vivo* Measurement of Human Skin Thermal Conductance Using a Calorimetric Sensor. *Journal of Thermal Analysis and Calorimetry*, **147**, 10027-10036. https://doi.org/10.1007/s10973-022-11275-x

55. Alberti-Fidanza, A., Burini, G., Perriello, G. and Fidanza, F. (2003) Trace Element Intake and Status of Italian Subjects Living in the Gubbio Area. *Environmental Research*, **91**, 71-77. https://doi.org/10.1016/s0013-9351(02)00016-6

56. Hatfield, H.S. and Pugh, L.G.C. (1951) Thermal Conductivity of Human Fat and Muscle. *Nature*, **168**, 918-919. https://doi.org/10.1038/168918a0

57. Robinson, M.P., Richardson, M.J., Green, J.L. and Preece, A.W. (1991) New Materials for Dielectric Simulation of Tissues. *Physics in Medicine and Biology*, **36**, 1565-1571. https://doi.org/10.1088/0031-9155/36/12/002

58. Raulin, C. and Karsai, S. (2011) Laser and IPL Technology in Dermatology and Aesthetic Medicine. Springer.

59. Williams, L.R. and Leggett, R.W. (1989) Reference Values for Resting Blood Flow to Organs of Man. *Clinical Physics and Physiological Measurement*, **10**, 187-217. https://doi.org/10.1088/0143-0815/10/3/001

Supplementary Information

S1. NUMERICAL SIMULATIONS AND *IN-VIVO* STUDY

S1.1. Physics and Thermal Equations

As previously mentioned, COMSOL Multiphysics® Software was used to solve both the heat transfer and electrical equations employed in these models. To study the interaction between the currents produced by RF and the tissue (dermis and adipose tissue), four physics are used: dynamics of electric currents, electrostatics, electromagnetic heating, and heat transfer in biomaterials.

1) *Equations for Dynamic Electric Currents*

In the frequency domain (AC current mode) and time dependent study types, dynamic formulas accounting for both conduction and displacement currents are used.

Combining the time-harmonic equation of continuity (1) with Equation (2) and generalizing to handle current sources, yields the following Equation (3):

$$\nabla \cdot J = \nabla \cdot \left(\sigma E + J_e\right) = -j\omega\rho \tag{1}$$

$$\nabla \cdot D = \rho \tag{2}$$

$$-\nabla \cdot \left(\left(\sigma + j\omega\varepsilon_0\right)\nabla V - \left(J_e + j\omega P\right)\right) = Q_j \tag{3}$$

where J is the current density, σ is the electrical conductivity, E is the electrical field, J_e is the external current density, j is the imaginary number, ω is the frequency used, ρ is the charge density, D is the electric flux density, ε_0 is the vacuum permittivity, V is the electric potential, Q is the charge and P is the electric polarization vector.

For the transient case, using the transient equation of continuity (4) and generalizing to handle current sources, the resulting equation becomes (5):

$$\nabla \cdot J = \nabla \cdot \left(\sigma E + J_e\right) = \frac{\partial \rho}{\partial t} \tag{4}$$

$$-\nabla \cdot \frac{\partial}{\partial t}\left(\varepsilon_0 \nabla V - P\right) - \nabla \cdot \left(\sigma \nabla V - J_e\right) = Q_j \tag{5}$$

2) *Electrostatics Equations*

Under static conditions, the electric potential, V, is defined by Equation (6). By combining this equation with the constitutive relationship (7) between the electric displacement D and the electric field E, it is possible to represent Gauss' law as the following Equation (8):

$$E = -\nabla V \tag{6}$$

$$D = \varepsilon_0 E + P = \varepsilon E = \varepsilon_0 \varepsilon_r E \tag{7}$$

$$-\nabla \cdot \left(\varepsilon_0 \nabla V - P\right) = \rho \tag{8}$$

This equation describes the electrostatic field in dielectric materials.

3) *Electromagnetic Heating*

The Electromagnetic Heating represents the electromagnetic losses, Q_e. This electromagnetic heat will be the heat source used in the heat transfer equation, coupling the electric equations with heat transfer in biomaterials. It is determined by (9):

$$Q_e = Q_{rh} + Q_{ml} \tag{9}$$

where the resistive losses Q_{rh} are defined as (10) and, in this case, magnetic losses Q_{ml} are equal to zero.

$$Q_{rh} = \frac{1}{2} Re\left(J \cdot E^*\right) \tag{10}$$

where J is the current density and E is the electrical field.

4) *Bioheat transfer module*

The heat transfer equation for biomaterials is defined as (13) using (11) and (12):

$$\rho C_p \frac{\partial T}{\partial t} + \nabla \cdot q = Q_e + Q_{bio} \tag{11}$$

$$q = -k\nabla T \tag{12}$$

$$Q_{bio} = \rho_b C_{pb} \omega_b \left(T_b - T\right) + Q_{met} \tag{13}$$

where ρ is the density of the tissue, C_p is the specific heat capacity of the tissue at constant pressure, k is the thermal conductivity of the tissue, T is the absolute temperature of the tissue, q is the heat flux by conduction in the tissue, ρ_b is the blood density, $C_{p,b}$ is the blood-specific heat capacity at constant pressure, ω_b is the blood perfusion rate, T_b is the arterial blood temperature, Q_{met} is the metabolic heat source and Q_e is the heat source provided by the electromagnetic heating.

To solve the equations, the thermal and electrical parameters of each of the tissues that make up the area to be treated must be known, as well as those of the materials used to manufacture the RF tips. The monopolar tips are capacitive electrodes fabricated from a resistive material (Aluminum 6082) but covered with a thin layer of an insulating material (Anodized Aluminum), thus, in addition to electrical resistance they also have a high electrical capacity. The bipolar tips are resistive electrodes made of a material that only has electrical resistance (Steel AISI 4340).

The thermal (**Table S1**) and electrical (**Table S2**) parameters of the tissues and materials used are shown, in addition to the thermal and perfusion parameters of the blood in the tissues (**Table S3**).

Table S1. Thermal parameters of the tissues and materials.

Thermal Parameters			
Material	ρ (kg/m^3)	k (W/m·K)	C_p (J/kg·K)
Skin	1030 [52]	0.376 [53]	3360 [54]
Fat (adipose tissue)	900 [55]	0.204 [56]	2430 [57]
Electrodes (Aluminum 6082) [Supplier]	2700	150	900
Electrodes (Stainless Steel) [Comsol]	7850	44.5	475

Table S2. Electrical parameters of the tissues and materials (* = dependent on the frequency "*f*" in Hz).

Electrical Parameters		
Material	σ(S/m)	ε_r
Skin [IFAC]*	$0.066\log(f) - 0.693$	$4768.48\exp\left(-\frac{f}{831049.64}\right) + 23874.76\exp\left(-\frac{f}{123720.74}\right) + 298.55\exp\left(-\frac{f}{28473910.75}\right) + 194.48\exp\left(-\frac{f}{302801677.8}\right)$

Continued

Fat (adipose tissue) [IFAC]*	$-8.07295\times10^{-30} f^4$ $+1.0408\times10^{-22} f^3$ $-4.24735\times10^{-16} f^2$ $+1.06893\times10^{-9} f$ $+0.025$	$27.09\exp\left(-\frac{f}{12017553.91}\right)$ $+176.23\exp\left(-\frac{f}{67339.16}\right)$ $+34.01\exp\left(-\frac{f}{368253.69}\right)$
Capacitive layer (Anodized Aluminum 30 um thick) [Supplier]	10^{-12} (Ohm·cm)	16.8
Electrodes (Stainless Steel) [Supplier]	4.032×10^6	1

Table S3. Thermal and perfusion parameters of blood.

Blood Parameters	
Parameter	**Value**
Arterial blood temperature (T_b)	310.15 (K)
Specific heat, blood ($C_{p,b}$) [58]	3.22 [J/(g·K)]
Blood perfusion rate for adipose tissue (ω_b) [59]	4.2×10^{-4} (1/s)
Blood perfusion rate for skin (ω_b) [59]	0.0018 (1/s)
Density, blood (ρ) [58]	900 (kg/m^3)

S1.2. Boundary Conditions

Thermal and Electrical Boundary Conditions Were Established

Thermal and electrical boundary conditions were established.

With regard to the electrical boundary conditions, first, the surfaces of application of an electric potential (electrodes) and the return surface ($V = 0$) can be distinguished. For a monopolar tip, the electrical potential application surface is the electrode surface, and the return surface is through a passive plate (for simplicity, a plane at infinity has been considered). In the case of the bipolar tip, the electrical potential application surface is the surface of one electrode row, and the return surface is the other row of electrodes. As an electric current source, a potential is applied. The equipment does not apply a specific power, but a potential difference, which, depending on factors such as the impedance adaptation or the electrical impedance of the tissue to be treated delivers a specific electrical power. The electrical power delivered heats the tissue depending on its electrical characteristics. Secondly, it is necessary to simulate the tissue edges. In this case, they are approximated by an infinite distance (infinite domains) to simulate that an electric current is applied to a tissue of dimensions much larger than the dimensions of the applicator. Lastly, all other external surfaces involved in the simulation are considered isolated from the outside, since in principle they are in contact with the air. The electrical initial conditions are 0 V in all the studied materials.

Regarding the thermal boundary conditions, the initial temperature for biological tissue was set at 36˚C (body temperature) and the surface of the electrode at a temperature between 27˚C and 29˚C, taken from the experiments carried out with the different electrodes. All other exterior surfaces are considered thermally insulated, which means that there is no heat flow in their contours. The heat source is the electric current that flows through the tissue. Therefore, it is a source of heat by volume, and is the result of the application of the electrical module on the biological tissue.

S1.3. Mesh Generation

Four mesh structures were used: extra fine for the contact surface between the dermis and electrodes, very fine for the dermis, fine for the electrodes and coarse for the adipose tissue.

S1.4. Pre-Clinical Study with *Ex Vivo* Tissue

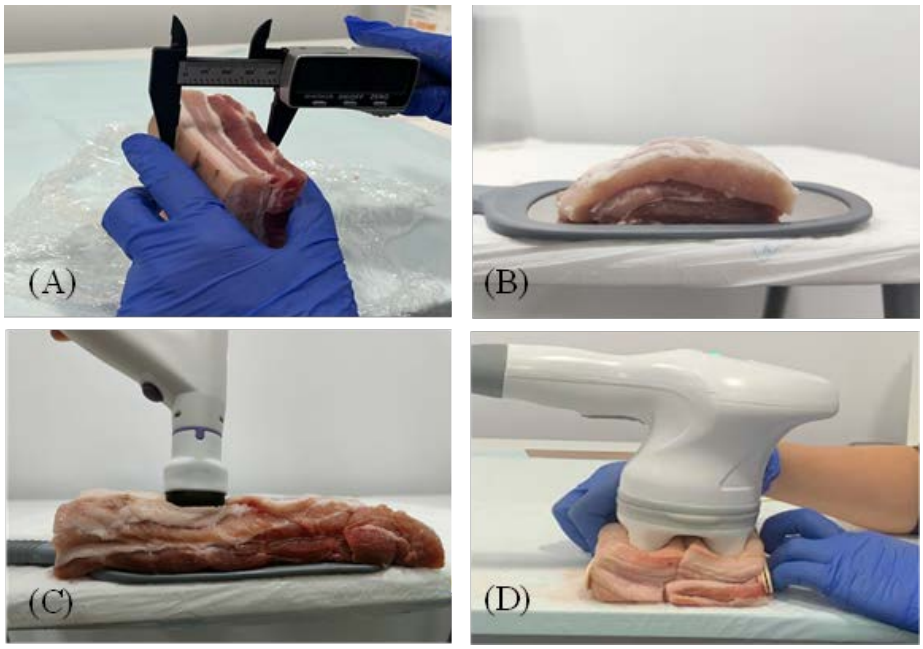

Figure S1. (A) Measurement of tissue thickness. (B) The tissue is placed on the passive plate if the test is conducted with monopolar tips. (C) Test with the monopolar Firm tip. (D) Test with the bipolar Sculpt6 tip; tissue cut in half to observe internal heating after the test.

S2. CLINICAL VALIDATION

S2.1. Clinical Treatments-Efficacy of S&S Tips for Skin Tightening and Body Contouring

Table S4. Patient information and clinical treatments.

Patient	Gender	Age	Sessions	Zone	Area	Tip	Frequency (MHz)	Time (min)
P1	Female	29	10	Body	Legs	Sculpt6	1	60
P2	Female	43	7	Facial	Neck	Firm	1	12
P3	Female	47	8	Facial	Face	Shine	1	24
P3	Female	47	8	Facial	Face	Firm	1	18
P4	Female	22	9	Body	Legs	Sculpt6	1	60
P5	Female	29	8	Body	Buttocks	Sculpt6	1	30
P6	Female	51	10	Facial	Face	Firm	1	18
P6	Female	51	10	Facial	Face	Shine	1	24
P6	Female	51	10	Body	Legs	Sculpt6	1	60

Continued

P7	Male	47	8	Facial	Face	Firm	1	18
P7	Male	47	8	Facial	Face	Shine	1	18
P8	Male	27	10	Body	Flanks	Sculpt6	0.5	20
P8	Male	27	10	Body	Abdomen	Sculpt6	0.5	20
P9	Female	29	8	Body	Legs	Sculpt6	0.5	60
P10	Female	44	8	Facial	Face	Firm	1	18
P10	Female	44	8	Facial	Face	Shine	1	24
P11	Female	47	9	Facial	Face	Firm	1	18
P11	Female	47	9	Facial	Neck	Firm	1	12
P11	Female	47	9	Facial	Face	Shine	1	18
P12	Female	44	9	Body	Abdomen	Sculpt6	1	20
P12	Female	44	9	Body	Legs	Sculpt6	1	60
P13	Female	50	8	Facial	Face	Firm	1	18
P13	Female	50	8	Facial	Neck	Firm	1	12
P13	Female	50	8	Facial	Face	Shine	1	24
P14	Female	52	9	Body	Legs	Sculpt6	1	60
P15	Female	60	8	Body	Décolletage	Firm	1	10
P16	Female	32	8	Body	Abdomen	Sculpt6	0.5	20